

Supporting Information for

One unprecedented 1-D europium thioindate-thioantimonate based on heterometallic mixed nitro-thiocusters with photoluminescent properties

Jian Zhou, Litao An, Xing Liu, Huahong Zou, Feilong Hu, Qiaomin Liu

General Remarks

All analytical grade chemicals were obtained commercially and used without further purification. Elemental analyses (C, H, and N) were performed using a PE2400II elemental analyzer. Energy-dispersive X-ray analysis (EDXA) was taken by using a JEOL JSM-6700F field-emission scanning electron microscope. FT-IR spectra were recorded with a Nicolet Magna-IR 550 spectrometer in dry KBr disks in the 4000-400 cm⁻¹ range. The UV/Vis spectra were recorded at room temperature using a computer-controlled PE Lambda 900 UV/Vis spectrometer equipped with an integrating sphere in the wavelength range of 190–2000 nm. Fluorescence spectral analyses were performed using a Cary Eclipse fluorescence spectrometer. Thermogravimetric analyses (TGA) were performed using a Mettler TGA/SDTA851 thermal analyzer under a N₂ atmosphere with a heating rate of 10 °C min⁻¹ in the temperature region of 25–500°C. Powder X-ray diffraction (XRD) patterns were collected on a D/MAX-3C diffractometer using graphite-monochromatized Cu K α radiation ($\lambda = 1.5406 \text{ \AA}$).

Crystal Structure Determination

Single-crystal X-ray diffraction data for **1** were recorded on a Rigaku Mercury CCD diffractometer using a ω -scan method with graphite monochromated Mo K α radiation ($\lambda = 0.71073 \text{ \AA}$) at 293(2) K to a maximum 2θ value (51.20°). Absorption corrections were applied using multi-scan technique. The structure of **1** was solved by Direct Method of SHELXS-97 and refined by full-matrix least-squares techniques using the SHELXL-97 program. Non-hydrogen atoms were refined with anisotropic temperature parameters. SIMU restraint prevents the thermal ellipsoids of all adjacent C and N atoms to adopt different orientations. All H atoms were positioned with idealized geometry and refined with fixed isotropic displacement parameters. According to the results of inductively coupled plasma and energy-dispersive X-ray analysis, the occupation factors of N18, N16-N17, and C25-C28 atoms were determined as 0.25, 0.5, and 0.5, respectively. Relevant crystal and collection data parameters and refinement results can be found in Table S1. Additional details of crystal data in CIF format can be found in the Supporting Information. Selected Bond Lengths (Å) and Angles (deg) for **1** are listed in Table S2.

Table S1 Crystallographic data for **1**.

1	
formula	C ₁₀₄ H ₃₀₇ Eu ₁₂ In ₁₆ N ₆₅ O ₄ S ₄₈ Sb ₄
Fw	8219.53
crystal system	monoclinic
space group	P2 ₁ /c
<i>a</i> , Å	15.167(3)
<i>b</i> , Å	28.929(6)
<i>c</i> , Å	15.709(3)
β, deg	111.35(3)
<i>V</i> , Å ³	6420(2)
<i>Z</i>	1
<i>T</i> , K	293(2)
Calcd density, Mg.m ⁻³	2.124
abs coeff, mm ⁻¹	5.135
<i>F</i> (000)	3922
2θ(max), deg	51.20
Total reflns collected	39589
Unique reflns	11700
No. of param	604
<i>R</i> 1[<i>I</i> >2σ(<i>I</i>)]	0.0843
<i>wR</i> 2(all data)	0.1718

Table S2. Selected Bond Lengths (Å) and Angles (deg) for **1**.

Sb1-S10	2.359(6)	Eu3-N6	2.570(18)
Sb1-S12	2.417(7)	Eu3-N9	2.582(16)
Sb1-S11	2.425(6)	Eu3-N8	2.62(2)

Sb1-Eu2	3.711(2)	Eu3-S12	2.831(6)
Eu1-N15	2.64(2)	Eu3-S11	2.947(6)
Eu1-N13	2.71(2)	In1-S4	2.436(6)
Eu1-N11	2.71(2)	In1-S2	2.448(7)
Eu1-N12	2.73(3)	In1-S1	2.499(6)
Eu1-N14	2.817(19)	In1-S3	2.504(6)
Eu1-S7	3.067(5)	In2-S2	2.417(6)
Eu1-S9	3.132(7)	In2-S7	2.448(7)
Eu1-S6	3.240(7)	In2-S6	2.452(5)
Eu1-In4	3.852(3)	In2-S5	2.506(9)
Eu1-In3	3.8880(19)	In3-S8	2.423(7)
Eu1-In2	3.902(2)	In3-S4	2.427(6)
Eu2-O1	2.338(13)	In3-S7	2.482(7)
Eu2-N1	2.484(18)	In3-S9	2.493(5)
Eu2-N5	2.547(18)	In4-S3	2.430(6)
Eu2-N3	2.582(19)	In4-S9	2.453(7)
Eu2-N4	2.604(17)	In4-S8#1	2.461(5)
Eu2-N2	2.651(16)	In4-S6	2.491(7)
Eu2-S10	2.871(6)	Eu3-O1	2.297(15)
Eu2-S11	2.924(6)	Eu3-N7	2.52(2)
Eu2-Eu3	3.9821(19)	Eu3-N10	2.527(17)
S10-Sb1-S12	103.9(3)	S4-In1-S2	107.2(2)
S10-Sb1-S11	95.9(2)	S4-In1-S1	104.6(2)
S12-Sb1-S11	94.2(2)	S2-In1-S1	106.7(2)
S10-Sb1-Eu2	50.66(15)	S4-In1-S3	117.3(2)
S12-Sb1-Eu2	82.78(19)	S2-In1-S3	117.1(2)
S11-Sb1-Eu2	51.91(15)	S1-In1-S3	102.5(2)
N15-Eu1-N13	117.0(7)	S2-In2-S7	111.3(2)
N15-Eu1-N11	68.6(8)	S2-In2-S6	120.7(2)
N13-Eu1-N11	106.1(8)	S7-In2-S6	106.2(2)
N15-Eu1-N12	126.1(8)	S2-In2-S5	106.8(3)
N13-Eu1-N12	65.7(7)	S7-In2-S5	107.7(3)
N11-Eu1-N12	60.3(7)	S6-In2-S5	103.3(2)
N15-Eu1-N14	68.6(6)	S8-In3-S4	111.88(19)
N13-Eu1-N14	60.4(6)	S8-In3-S7	103.0(2)
N11-Eu1-N14	118.8(7)	S4-In3-S7	118.6(2)
N12-Eu1-N14	122.8(7)	S8-In3-S9	109.0(2)
N15-Eu1-S7	107.6(5)	S4-In3-S9	110.7(2)
N13-Eu1-S7	134.3(5)	S7-In3-S9	103.00(19)
N11-Eu1-S7	80.2(5)	S3-In4-S9	116.6(2)
N12-Eu1-S7	80.5(5)	S3-In4-S8#1	116.7(2)
N14-Eu1-S7	154.5(5)	S9-In4-S8#1	104.4(2)
N15-Eu1-S9	146.1(6)	S3-In4-S6	107.0(2)
N13-Eu1-S9	71.2(5)	S9-In4-S6	107.1(2)
N11-Eu1-S9	143.7(5)	S8#1-In4-S6	104.0(2)
N12-Eu1-S9	87.7(5)	O1-Eu3-N7	148.5(6)

N14-Eu1-S9	92.0(5)	O1-Eu3)-N10	83.4(6)
S7-Eu1-S9	77.83(15)	N7-Eu3-N10	83.3(6)
N15-Eu1-S6	71.9(6)	O1-Eu3-N6	83.7(6)
N13-Eu1-S6	125.7(5)	N7-Eu3-N6	65.4(6)
N11-Eu1-S6	124.9(6)	N10-Eu3-N6	75.6(5)
N12-Eu1-S6	154.9(5)	O1-Eu3-N9	90.2(5)
N14-Eu1-S6	78.2(5)	N7-Eu3-N9	108.7(6)
S7-Eu1-S6	76.75(15)	N10-Eu3-N9	63.0(5)
S9-Eu1-S6	77.23(17)	N6-Eu3-N9	138.6(5)
O1-Eu2-N1	78.0(4)	O1-Eu3-N8	146.7(6)
O1-Eu2-N5	79.9(5)	N7-Eu3-N8	64.7(6)
N1-Eu2-N5	94.1(6)	N10-Eu3-N8	106.5(6)
O1-Eu2-N3	152.3(5)	N6-Eu3-N8	129.4(6)
N1-Eu2-N3	127.4(5)	N9-Eu3-N8	67.9(6)
N5-Eu2-N3	86.7(6)	O1-Eu3-S12	94.3(3)
O1-Eu2-N4	85.5(5)	N7-Eu3-S12	81.5(4)
N1-Eu2-N4	154.9(6)	N10-Eu3-S12	146.2(4)
N5-Eu2-N4	64.2(5)	N6-Eu3-S12	70.7(4)
N3-Eu2-N4	66.8(5)	N9-Eu3-S12	150.7(4)
O1-Eu2-N2	131.9(5)	N8-Eu3-S12	93.9(4)
N1-Eu2-N2	63.0(5)	O1-Eu3-S11	73.8(4)
N5-Eu2-N2	76.2(6)	N7-Eu3-S11	133.7(5)
N3-Eu2-N2	66.3(5)	N10-Eu3-S11	134.4(4)
N4-Eu2-N2	118.9(6)	N6-Eu3-S11	137.6(3)
O1-Eu2-S10	125.3(4)	N9-Eu3-S11	77.9(4)
N1-Eu2-S10	78.7(4)	N8-Eu3-S11	77.1(4)
N5-Eu2-S10	150.5(4)	S12-Eu3-S11	75.70(19)
N3-Eu2-S10	75.8(5)	N5-Eu2-S11	131.2(3)
N4-Eu2-S10	126.4(4)	N3-Eu2-S11	98.2(4)
N2-Eu2-S10	75.0(5)	N4-Eu2-S11	73.4(4)
O1-Eu2-S11	73.7(4)	N2-Eu2-S11	149.4(4)
N1-Eu2-S11	118.7(5)	S10-Eu2-S11	75.62(17)

Symmetry transformations used to generate equivalent atoms:

(#1) $x, -y+1/2, z-1/2$.

Table S3. Hydrogen bonds for **1** [Å and deg].

D-H…A	d(D-H)	d(H…A)	d(D…A)	\angle (DHA)
N3-H3C…S10	0.91	2.93	3.36(2)	110.2
N5-H5C…S4#1	0.90	2.50	3.395(19)	173.8
N5-H5D…S6	0.90	3.00	3.77(2)	143.7
N6-H6C…S12	0.90	2.71	3.131(18)	110.1
N6-H6D…S3#1	0.90	2.62	3.47(2)	158.4
N7-H7C…S2#2	0.91	2.67	3.491(18)	151.2
N9-H9C…S5#3	0.91	2.77	3.57(2)	147.1
N10-H10D…S3#1	0.90	2.91	3.81(2)	175.1
N11-H11D…S12#4	0.90	2.61	3.46(3)	158.4

N12-H12C···S8	0.91	2.81	3.66(2)	155.2
N13-H13C···S9	0.91	2.80	3.42(2)	126.0
N14-H14C···S8#1	0.91	2.55	3.42(2)	160.0
N15-H15C···N11	0.90	2.57	3.02(3)	111.5
N15-H15C···S11#3	0.90	2.83	3.50(2)	131.9
N15-H15D···S6	0.90	3.02	3.49(3)	114.2

Symmetry transformations used to generate equivalent atoms: (#1)
 $x, -y+1/2, z-1/2$; (#2) $x, y, z-1$; (#3) $-x+1, -y, -z+1$; (#4) $x+1, y, z+1$.

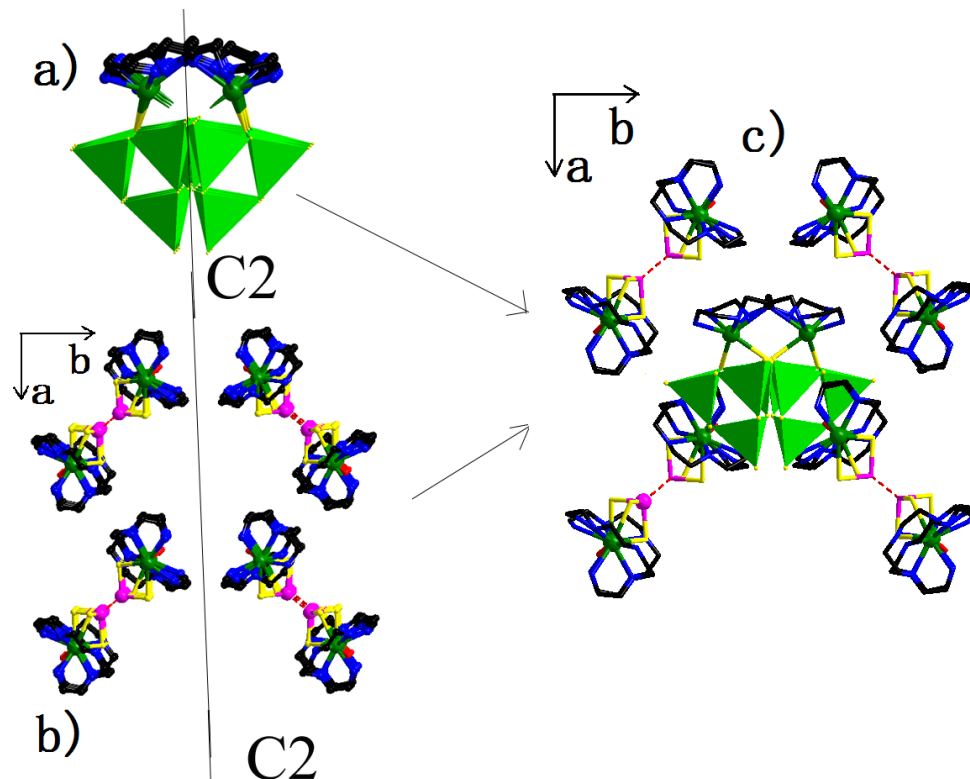


Figure S1 Representations of the host-guest symmetry in **1**. a) The view of the 1-D $[\text{Eu}(\text{tepa})\text{In}_4\text{S}_9^{3-}]_n$ chain along the axial direction, b) the pseudo-channel with the C_2 symmetry, c) the 1-D $[\text{Eu}(\text{tepa})\text{In}_4\text{S}_9^{3-}]_n$ chains located at the pseudo-hexagonal channel.

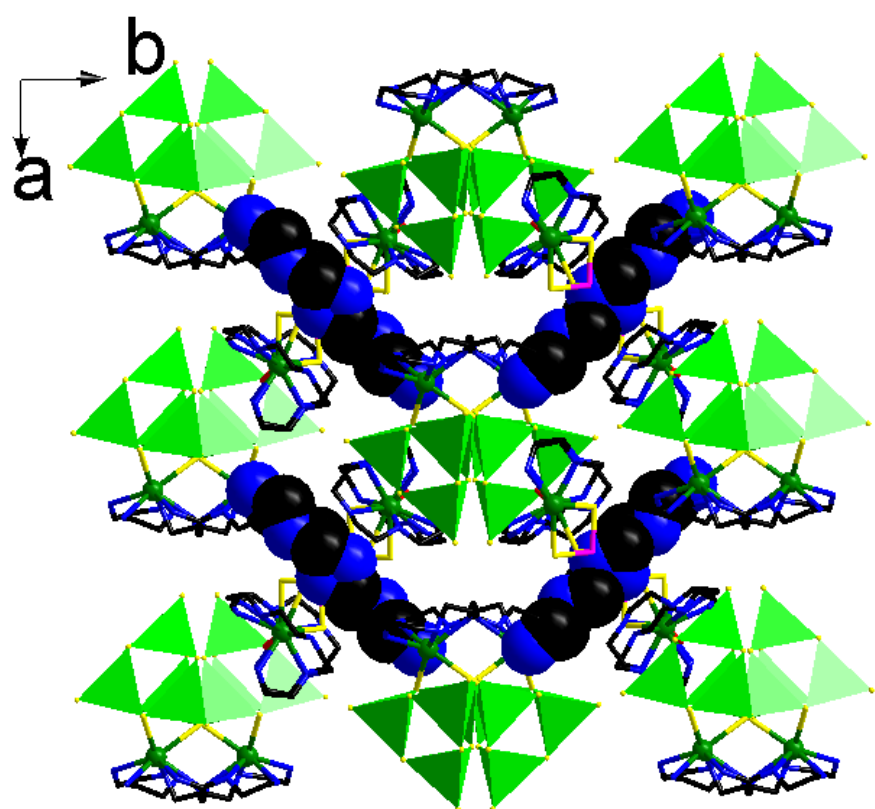


Figure S2 Crystal packing of **1**. All H atoms are omitted for clarity.

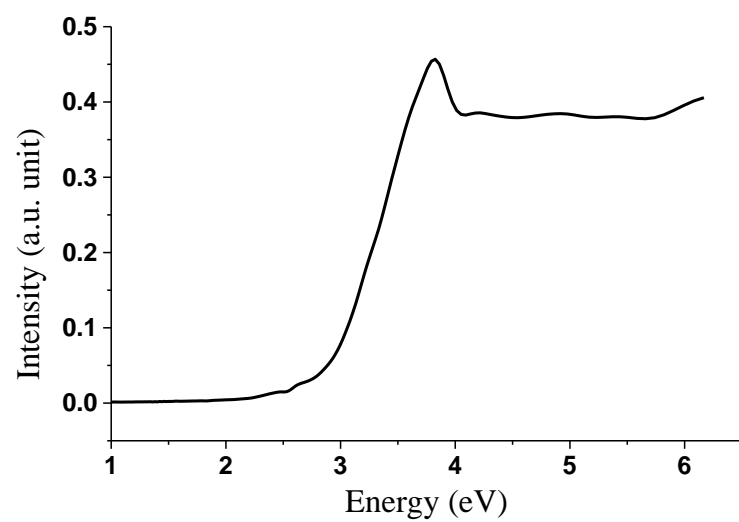


Figure S3 Solid-state optical absorption spectrum of **1**.

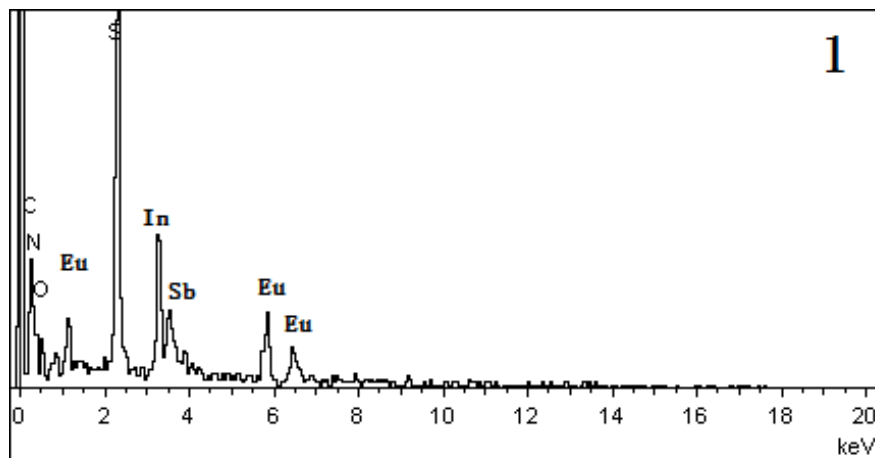


Figure S4. EDS spectrum of **1**.

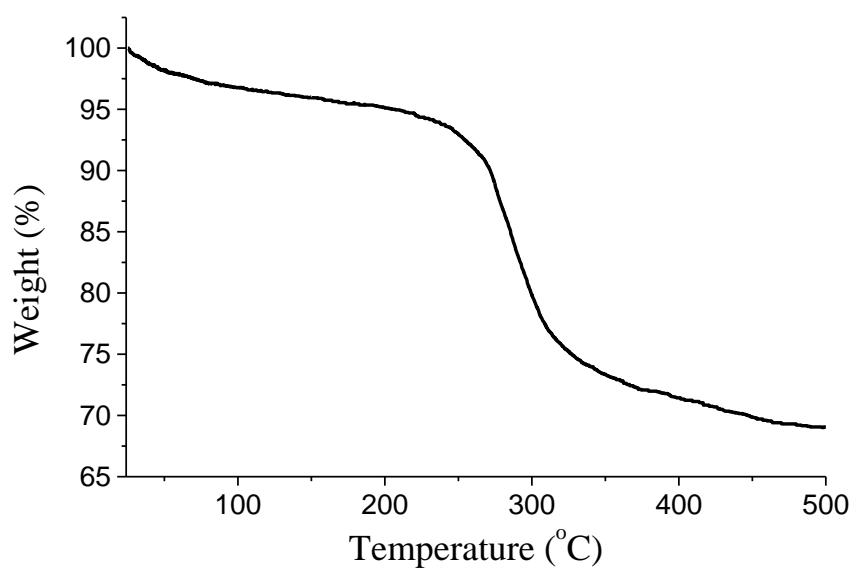


Figure S5 TG curve of **1**.

The TG curve shows that one-step weight losses (30.67 %) occur in the range of 25-450 °C, assigned to the removal of the H₂O molecules and decomposition of organic species (calcd 30.82 %).

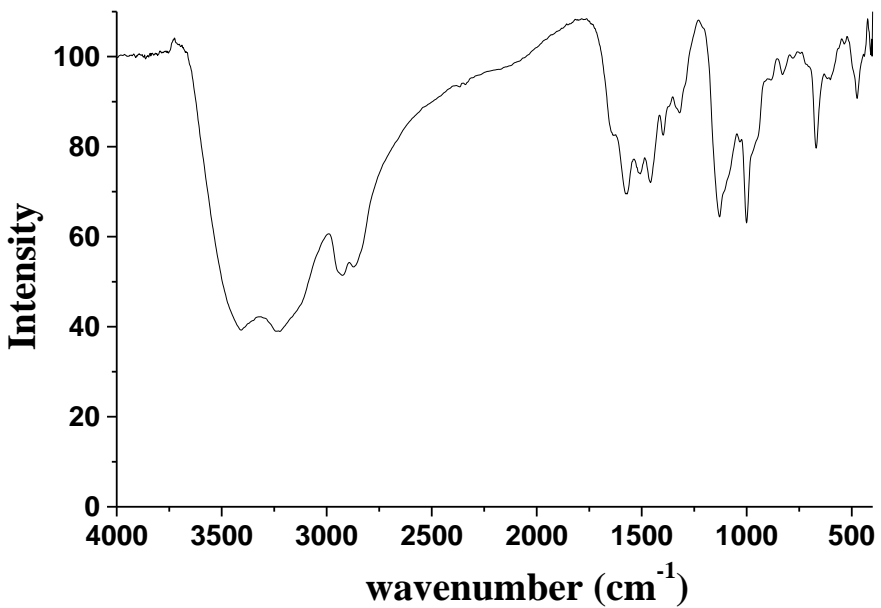


Figure S6 IR spectrum of **1**.

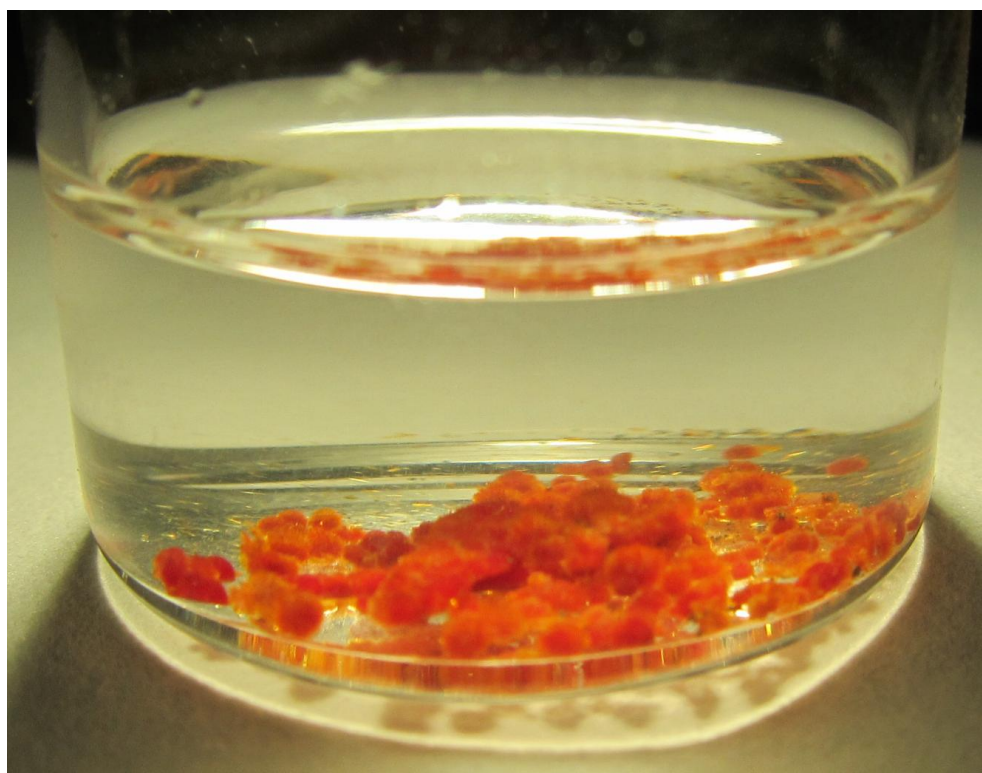


Figure S7 Photo of the crystals of **1** at ambient condition.

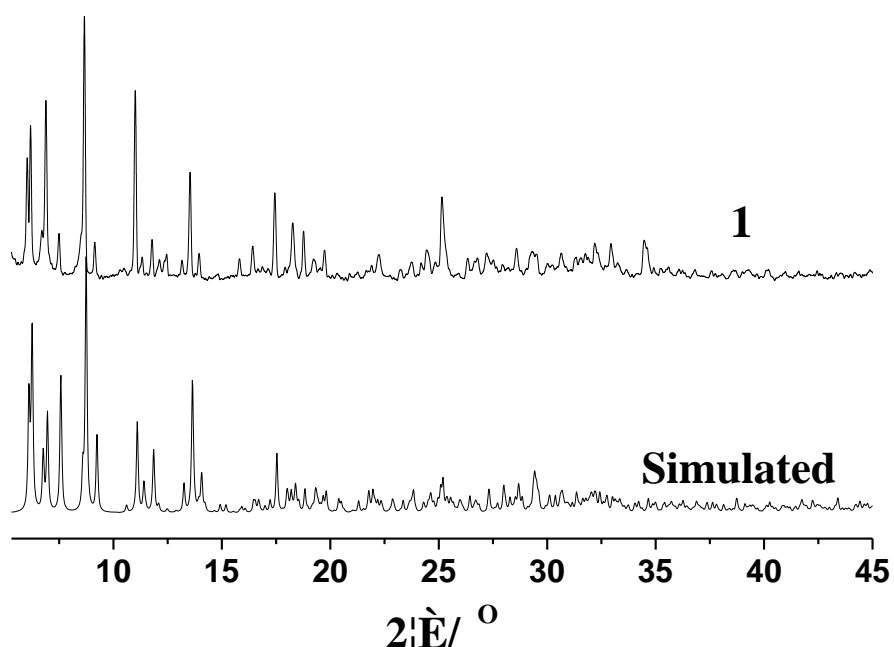


Figure S8 Simulated and experimental powder XRD patterns of **1**.

The experimental peak positions are in agreement with simulated XRD pattern, indicating the phase purity of **1**. The difference in reflection intensity between experimental and simulated XRD patterns is probably due to the preferred orientation effect of the powder sample during collection of the experimental XRD data.